Modeling Emission Features of Salicylidene Aniline Molecular Crystals: a QM/QM' Approach

Davide Presti[1], Frédéric Labat[2], Alfonso Pedone[1,], Michael J. Frisch[3], Hrant P. Hratchian[4]

Ilaria Ciofini[2], Maria Cristina Menziani[1] and Carlo Adamo[2,5]

[1]*Dipartimento di Scienze Chimiche e Geologiche, Università di Modena e Reggio-Emilia, 103 via G. Campi, I-41125 Modena, Italy.*

[2]*Institut de Recherche de Chimie Paris CNRS Chimie ParisTech, 11 rue P. et M. Curie, F-75005 Paris 05, France.*

[3]*Gaussian, Inc. 340 Quinnipiac St., Bldg. 40 , Wallingford, CT 06492, USA*

[4]*Chemistry and Chemical Biology, University of California, Merced, CA 95343.*

[5]*Institut Universitaire de France, 103 Boulevard Saint Michel, F-75005 Paris, France.*

*Corresponding Authors: alfonso.pedone@unimore.it; carlo.adamo@chimie-paristech.fr

Abstract

A new computational protocol is proposed to compute the emission spectra of molecular crystal and applied to the β-form of salicylidene aniline (SA).

The first singlet excited states (S_1) of the SA cis-keto and trans-keto conformers, surrounded by a cluster of other molecules representing the crystalline structure, were optimized by using a QM/QM' ONIOM approach with and without electronic embedding. The model system consisting of the central salicylidene aniline molecule was treated at the DFT level by using either the B3LYP, PBE0, or the CAM-B3LYP functionals, whereas the real system was treated at the HF level.

The CAM-B3LYP/HF level of theory provides emission energies in good agreement with experiment with differences of -20/-32 nm (**cis-keto** form) and -8/-14 nm (**trans-keto** form), respectively, whereas notably larger differences are obtained using global hybrids.

Though such differences on the optical properties arise from the density functional choice, the contribution of the electronic embedding is rather independent by the functional used. This supports a more general applicability of the present protocol to other crystalline molecular systems.

Keywords : DFT, TD-DFT, molecular crystals, ONIOM QM/QM', photophysics

1. Introduction

Molecular crystals represent a class of advanced materials widely employed in photonic and optoelectronic applications.[1]–[6] Many of these belong to the family of *photo*- (PC) or *thermo-chromic* (TC) materials that is, systems that change their color after photo- or thermo- irradiation, respectively.[3], [4] This *reversible* process is always associated to a structural change that in the solid-state affects, beyond molecules, also the crystalline structure.

Notwithstanding the photophysical processes are largely investigated both at the experimental and computational level on single molecules, the number of corresponding studies on molecular crystals in the solid state is still rather poor.

In this context, the Salicylidene Aniline (SA) molecule, which is the precursor of all aromatic Schiff bases, attracted the attention of many experimental investigations because of its peculiar optical properties, which stem from a fast excited-state intramolecular proton transfer (ESIPT) reaction, that also takes place within the solid, and from a cis-to-trans keto isomerization.[7]–[21]

The PC/TC mechanism of the SA molecule in gas-phase and in solution involves several steps[20] , as reported in Figure 1. Firstly, the stable enol form (nonplanar in solution) is promoted, under irradiation, to the excited state, where it assumes a quasi-planar (cis-enol) conformation. Then, the SA molecule undergoes an ESIPT that transforms it from the colorless enol to the colored (yellow-orange) cis-keto form. At this point, the cis-keto form can either relax back to the ground state (enol form), or it can switch to the trans-keto form (orange-red) by cis-keto tautomerization, and successively relax to the enol form.

Very little is known about this mechanism in the solid state. Difficulties in the experimental investigation of SA polymorphs brought only to disclose two PC structures, namely α_1[22], [23] and α_2,[23], [24] and one TC structure – the β[23] polymorph for the enol form in the ground state. Even after the structural revision provided by Arod et al [23] comprehensive experimental studies of PC/TC properties of crystalline SA are still not available. The only additional information provided by the results reported by these authors [23] is that SA is always almost planar, both in the ground state and in the excited state.

Focusing on the emission properties, to the best of our knowledge only few experimental molecular data are available,[7], [18], [20], [25] for the emission features of SA, and only one study of steady-state fluorescence was carried out in solid-state.[17] In this latter, a keto fluorescence emission was observed (λ_{max} ~ 541 nm), without a clear distinction between the

molecular cis- and trans- keto forms. Moreover, the ground-state was indicated as 'photochromic', but this was prior to the last revision of the experimental structures by Arod et al.[23]

A possible solution to gain insights is to resort to modern computational tools, such as Density Functional Theory (DFT) and Time-Dependent-DFT, that can reliably provide both ground and excited state properties of molecules in solutions and in the solid state.[26]–[33]

Quantum mechanical calculations have been already employed to simulate the optical properties of SA in gas-phase and in various solvents,[21], [34]–[36] as well as the complex dynamics of the PC gas-phase process,[36] whereas the same properties in solid-state have been only partially addressed by experimental works.[15], [17], [19]

In a recent paper,[37] we employed TD-DFT calculations in order to simulate the optical absorption properties of the β thermochromic polymorph of SA (depicted in Figure 2). A computational protocol was established and adopted to compute, with good accuracy, the vertical excitation energies associated to the UV-Visible absorption of crystalline SA.

Such protocol consisted of: i) obtaining a reliable ground-state geometry – full relaxation – of the stable crystal (enol form), by adopting dispersion-corrected DFT approaches (i.e. B3LYP-D* [38]) within periodic boundary conditions (PBC); ii) defining a subsystem (cluster of molecules) representative of the infinite solid, through the careful analysis of the most relevant intermolecular structural parameters; iii) further optimizing the central molecule of SA – in the enol, cis-keto and trans-keto forms – within a cluster of fourteen surrounding molecules always fixed in the enol form finally getting three clusters : the **C-enol** (Figure 2), the **C-cis-keto** and the **C-trans-keto** (Figure 3), respectively. Point iii) was carried out assuming that the thermochromic process does not take place for all molecules simultaneously. Next, iv) the study of the absorption features of the clusters was carried out by using the QM/QM' ONIOM approach combined with an electronic charge embedding model.[39], [40] The latter allowed an improved description of the environmental effects on the central molecule of SA, demonstrating that such protocol can be applied to predict safely the UV-Visible absorption properties of solid SA by substituting the periodic crystal with the mentioned clusters.

With the present work, some theoretical insights into the emission features (fluorescence) of thermocromic SA are provided, through the adoption of the protocol summarized above, and the effects of a charge embedding model on electronic and optical features are addressed. This task is

accomplished by taking into account the procedures adopted to compute the SA absorption properties.[37] The details concerning the computational setup are discussed in the next Section.

In Section 'Results and Discussion', the structural parameters of the thermochromic polymorph of SA are discussed briefly, whereas the intramolecular ones are compared between various forms of SA. Then, the calculated vertical emission energies and the behavior of simulated fluorescence emission spectra are discussed in relation to the: a) structure and relative stability of SA in different aggregation states (gas-phase, solvent, clusters); b) choice of different density functional approximations; d) structural and electronic effects of charge embedding on clusters; e) overall accuracy of absorption and emission for cluster calculations (QM/QM' + charge embedding), according to experiment.

Finally, some conclusions on the modeling of emission features of SA are exposed, as well as some perspectives on the general applicability of our protocol to molecular crystals together with possible ways improvement.

2. Computational Details

The development version of Gaussian09[41] was employed for all calculations. This program makes use of atom-centered gaussian-type orbitals (GTO) as basis-sets.

QM/QM' cluster calculations. The **C-cis-keto** and **C-trans-keto** clusters were extracted from the bulk structures optimized at the B3LYP-D* level of theory in a previous paper[37] by using the CRYSTAL code.[42], [43] The starting input geometries are reported in Tables S1.A and S1.B of Supporting Information.

In order to investigate the absorption and emission features of thermochromic SA, the ground (S_0) and first singlet excited state (S_1) of the **C-cis-keto** and **C-trans-keto** clusters were optimized by using a QM/QM' ONIOM protocol. The model system consisting of the central SA molecule was treated at the DFT level by using either the B3LYP[44], PBE0,[45] or the CAM-B3LYP[46] functionals in combination with the 6-31+G(d) basis set. The CAM-B3LYP functional has been used because it better reproduces charge transfer (CT) states.[47]–[49] The second (QM') layer is composed by 14 SA molecules frozen in their enol form and it was treated at the Hartree-Fock/STO-3G level of theory.

Within these two clusters, the optimization of the central (cis-keto/trans-keto) molecule was performed using a mechanical embedding ONIOM approach, whereas vertical emission energies were computed on the same systems using a (Mulliken[50]) charge embedding[39] scheme.

Calculations on isolated molecules. Vertical transition energies for the emissive forms (cis-keto and trans-keto) of molecular SA were also computed. The two structures, already optimized at their electronic ground state,[37] were taken as input (note that, in agreement with previous calculations,[34], [36]the optimization of the excited enol form of SA does not lead to a stable minimum, because it evolves to the cis-keto form).

A TD-DFT full relaxation of the first singlet excited state was carried out at the CAM-B3LYP/6-31+G(d) level of theory. Then, B3LYP/6-31+G(d) and PBE0/6-31+G(d) vertical emission energies were obtained as single point energies on the CAM-B3LYP geometry. This two step procedure was applied since a direct TD-DFT optimization with global hybrid functionals leads to convergence instabilities due to the presence of an over-stabilized intruding Charge Transfer state.

Calculations were carried out in gas-phase and in acetonitrile solvent (ACN). The latter was chosen for purposes of comparison with previous calculations[37] and with available experimental data.[17], [18], [20] The Conductor-like Polarizable Continuum Model[51] (C-PCM) was used to implicitly model solvent effects.

All Gaussian convoluted simulated spectra, obtained from computed vertical emission energies, were produced with an in-house code, by setting to 0.15 eV the full-width at half-maximum (FWHM) of each Gaussian function associated to the vertical transitions. Orbital surfaces were plotted adopting an isosurface density value of 0.02 a.u.

3. Results and Discussion

3.1 Structures of the β polymorph of SA, isolated molecules and clusters.

The thermochromic β polymorph structure of SA belongs to the orthorhombic *P*bc2_1 space group (details on lattice parameters are in given in Table S2 of Supporting Information), it is characterized by the presence of four molecules (Z=4) of SA in the unit cell, that lie along the *b* lattice vector and that are stacked along *c*, where the presence of dispersive interactions is more evident with respect to other directions. This kind of molecular displacement originates a 'fishbone'-like pattern on the *ab* plane, visible in Figure 2).

In both solid-state and isolated molecules, the enol and cis-keto forms of SA are characterized by one *intra*molecular hydrogen bond. Such feature is involved in the ESIPT process, and is obviously lost when the cis-trans (keto) tautomerization occurs upon rotation about the C7-C8 double bond (according to the labeling of Figure 1).

Figure 3 reports the optimized (CAM-B3LYP) excited state structures of the **C-cis-keto** and **C-trans-keto** clusters. A deep analysis of intermolecular interactions of these clusters in the ground state was already reported.[37] Moreover, excited-state forms are experimentally metastable (in fact, no structural data is available), therefore only intramolecular parameters are commented in the following. Those related to dihedral angles, however, can indirectly reflect the different effect of ACN solvent and crystalline environment on the SA molecule.

3.2 Structural differences between ground and excited state structures. Table 1 lists several intramolecular distances and angles computed for the two keto tautomers (cis and trans) in gas-phase and in ACN. These, when possible, are compared with high-level computational predictions from previous studies.[34], [36]

At the excited state, the bond distances predicted in the gas phase by CIS[34] and OM2/MRCI[36] for the cis-keto form are in fair agreement with the CAM-B3LYP calculations of the present study. However, less constrained parameters, as those related to the mutual rotation of aromatic moieties around the C6-N-C7-C8 dihedral angle, the C-O···H angle, and the O···H distance show more marked deviations, as expected. It is worth noting that C6-N-C7-C8 (labeled C6-N7-C8-C9 in Ref.[36]), unconstrained during optimization, does not result in a perfectly planar (180°) dihedral angle, as in previously published data.[34], [36]

In particular, for the trans-keto form a stable non-planar configuration in gas-phase (C6-N-C7-C8: -169.27°) was obtained here. Such configuration is not present among the OM2/MRCI structures proposed by Spörkel et al.,[36] due to an intermediate state between the cis-keto and the trans keto forms, found at the S_1/S_0 conical intersection of the two potential energy surfaces.

The comparison between each S_1 keto tautomer (CAM-B3LYP) with the corresponding one at the S_0 B3LYP geometry (last column of Table 1) shows that only minor variations occur, except for the dihedral angles, and the C-O···H angle of the trans-keto form. These latter are, in fact, more affected due to a larger number of degree of freedom with respect to other intramolecular parameters. The same trend, notably less evident, results from the set of calculations in ACN solvent. However, the reader should notice that the same difference (ca. 3°) is found between the

cis-keto and the trans-keto C5-C6-N-C7 dihedrals both in the S_1 and the S_0 states, but the former ones are more constrained to a planar configuration. This could result from consistent direct and indirect polarization effects induced by the solvent during geometry optimization (ACN has a rather high dielectric constant, $\varepsilon = 35.688$).

The calculated intramolecular parameters of molecular SA within cluster structures are reported in Table 2. A notable change in the C5-C6-N-C7 dihedral angle of +22°/+23° is observed for the excited state geometry of the **C-cis-keto** form with respect to the B3LYP-D* ground state geometry. For the **C-trans-keto** form, the same parameter, even retaining molecular planarity with respect to the input structure (C5-C6-N-C7 dihedral angle of -178.12°), results in major differences when global hybrids are adopted (B3LYP angle: +8.86° ; PBE0 angle: +9.92°). The use of CAM-B3LYP, instead, preserves SA from marked changes (angle of +3.43°) with respect to the B3LYP-D* starting configuration. Such differences highlight the structural effects on the S_1 state caused by the choice of the density functional approximation.

A quantitative structural relationship among different aggregation states of SA at the emission geometry is provided in Table 3, by considering the absolute differences between computed intramolecular parameters of SA in ACN and within clusters, with respect to the gas-phase, taken as reference. It turns out that the **C-cis-keto** cluster and the corresponding solvated form of SA optimizations lead to similar deviations, whereas for the trans-keto form the influence of different surrounding environments becomes more important. This is true even though electronic embedding (cluster calculations) is not introduced at this point: mechanical embedding effects are, nonetheless, present.

3.3 Relative stabilities. At this point, it becomes interesting to analyze another aspect which is influenced by structural and electronic features of SA: the relative stability of the two cis-keto tautomers at the S_1 optimized geometry. This is computed as $\Delta E_{cis\text{-}trans} = E_{cis} - E_{trans}$ and the values are reported in Table 4. Based on experimental evidences, it has been hypothesized that the cis-keto tautomer is less stable than the trans-keto one, both in gas-phase and in solution[20]. However, this is not undoubtedly proven, as the energy difference between the two minima on the potential energy surface (PES) can be very small. Overall, the results show that the cis-keto form is slightly more stable than the trans-keto form of a few kcal/mol. Structural effects on energy are highlighted by the variations in the cis-trans relative stability between different phases of SA, for the same density functional used, showing the same trend for all functionals.

Though this could be a consequence of the fact that B3LYP and PBE0 results are obtained from single point calculations performed on CAM-B3LYP optimized structures, some sizeable changes in energy are indeed present, and these could be a clue of the dependence of the relative stability on the density functional approximation employed.

More interestingly, the inclusion of electronic embedding on clusters calculations provides a practically constant contribution to the stabilization energy (<2 kcal/mol) and seems less dependent on the density functional approximation applied. Indeed, in this case there could be a balancing effect between the polarization on the central SA molecule (the latter changes between cis- and trans-keto forms, but the environment is always in the enol form, with HF Mulliken charges) and the response to the polarization field of the high-level QM layer.

3.4 Emission features. Table 5 reports the computed fluorescence emission energies ($S_1 \rightarrow S_0$) of SA in gas-phase, in ACN and in the different clusters. The emission energies of the trans-keto form is red shifted of about 50-80 nm with respect to those of the cis-keto form in both the gas-phase and in ACN, whereas such difference is less evident in cluster calculations (15-20 nm).

Assuming that these latters represent a suitable model to study emission in the molecular crystal, it may be noticed how difficult is to distinguish experimentally the two keto forms in the solid state, where the electronic transitions (λ_{max}) are convoluted into a broad gaussian band that spans from ca. 400 to 700 nm.[17]

It is worth noting that in the study by Ziółek et al.[17] the emissive keto tautomer (cis- or trans-) is not defined. Also, the polymorph nature of the emissive excited state forms is not clear (and the ground-state 'photochromic' form cannot be addressed to the last structural revision of Ref.[23]).

In Table 5, the experimental datum (541 nm, indicated in literature as 18500 cm^{-1}) and the related differences with respect to both the **C-cis-keto** and **C-trans-keto** cluster calculations are thus reported.

The simulated spectra reported in Figure 4 reveal that charge embedding effects produce some variations on the emission features of cluster systems, but do not dominate over the structural ones. This is partly ascribable to the fact that i) environmental effects were evaluated on the same optimized geometries of calculations without charge embedding; ii) the same level of theory (HF/STO-3G) is always used for the calculation of QM charges of the surrounding environment.

However, in agreement with vertical excitation (absorption) energies,[37] it is clear that structural changes act oppositely with respect to electronic effects: in the first case a redshift is observed,

going from the solvated molecule to clusters, whereas in the second case, i.e. by introducing charge embedding in cluster calculations, a blueshift is observed.

Still regarding the results on cluster calculations *without* and *with* charge embedding, ONIOM results obtained at the CAM-B3LYP/HF level always provide emission energies in good agreement with experiment (even if this latter cannot be assigned to the cis- or to the trans-keto form, as discussed above) with differences of -20/-32 nm (**C-cis-keto**) and -8/-14 nm (**C-trans-keto**), respectively, whereas notably larger differences are furnished by B3LYP/HF (Min.dev.: +107 nm, C-trans-keto/embedding; Max.dev.: +143 nm, C-cis-keto/no-embedding) and PBE0/HF (Min.dev.: +71 nm, C-trans-keto/embedding; Max.dev.: +103 nm, C-cis-keto/no-embedding). This highlights the effect of the density functional choice within the QM/QM' protocol: the change in emission maxima are similar for the two global hybrids adopted in the present work, B3LYP and PBE0. Instead, the CAM-B3LYP spectrum presents a different general trend and, with respect to B3LYP and PBE0, its cluster emission bands are *hypsochromically compressed* towards the ACN and gas-phase bands.

Furthermore, no functionals give satisfactory predictions (a general blueshift is observed with respect to experiment) for the cis-keto form in ACN solvent (-63 to -82 nm). However, it is also expectable that a little amount of cis/trans- keto interconversion and coexistence takes place experimentally, especially in solution.

Finally, the normalized intensity of SA emission in ACN solvent is always markedly higher (two to three times) than those associated to the other phases. This higher intensity of oscillator strengths (see Table S3 of Supporting Information) could either be caused by polarization effects or, more trivially, by the fact that calculations performed with explicit surrounding molecules are herein compared with those carried out with the implicit solvent (PCM method). It would be interesting, as a future work, to investigate such aspect, as well as the relationship between density functional choice and solvatochromic effects.

The differences between λ_{max} of trans- and cis- keto forms, depicted in Figure 5, display intuitively the amount of redshift produced by the cis-keto tautomerization process. Again, a similarity between B3LYP and PBE0 is observed, albeit a slightly larger difference between gas-phase structures (red bars) is given, whereas CAM-B3LYP produces analogous redshifts for ACN and gas-phase calculations. This is in agreement with that discussed in the case of structural parameters (as reported in Table 2). Nonetheless, it is evident that the small effect of charge

embedding (green vs. violet bars) makes the clusters calculations more sensitive to the type of density functional approximation used. Calculations performed at PBE0 and B3LYP on clusters show, when charge embedding is introduced, a blueshift of about 20 nm toward the experimental λ_{max} (see Table 5). However, the computed emission energies are still quite far from the experimental value. The results obtained at CAM-B3LYP level instead, with errors ranging from -20/-8 nm to -32/-14 nm with respect to experiment, are globally in fair agreement with it.

Table 5 also reports the character associated to the computed first singlet excited states. In the case of B3LYP and PBE0 results, the trans-keto forms present some relevant mixing of HOMO–LUMO and HOMO-1–LUMO one-electron excitations to the electronic state, except in the case of calculations performed in solvent, which presents a pure HOMO-LUMO character.

The orbitals involved are displayed in Figure 6 in the case of B3LYP gas-phase calculations, the two other exchange correlation functionals providing practically identical pictures, as reported in Figures S1 and S2 in Supporting Information). Cis- and trans- keto orbitals do not present marked differences, besides those obviously due to the different molecular geometry. In more details, HOMO and LUMO are of π and π^* type, respectively, and they are delocalized over the whole molecule, with a sizable localization of the HOMO on the phenolic ring. The trans-keto HOMO-1 orbital instead is fully localized on the phenolic ring and of σ type. As a consequence, the larger contribution of the HOMO-1 to LUMO excitation to the transition in the case of global hybrid functionals somehow increases the charge transfer character associated to this transition.

In order to better evaluate the impact of the exchange correlation functional used on the computed photophysical properties, the absorption and emission bands computed for all models are gathered in Figure 7. All vertical excitation energies and oscillator strengths are reported in Tables S11 and S12 of Supporting Information. These electronic transitions were calculated at the CAM-B3LYP, B3LYP and PBE0 level of theory on the clusters (for both keto tautomers) at the QM/QM' level including a charge embedding model.

It can be noticed that PBE0 and B3LYP perform better than CAM-B3LYP in describing vertical excitations, as they are closer to the experimental values of λ_{max} for absorption (cis-keto: 443 nm; trans-keto: 487 nm). However, both the cis- and trans- bands, as for CAM-B3LYP, are close to each other, and do not reflect the difference between experimental λ_{max} values. This behavior, though less pronounced, can be noted also for emission bands. A possible explanation can be found in the presence of SA molecules fixed in the enol form, as surrounding environment, in all

cases. As already stated,[37] in fact, the cluster model certainly represents a 'nucleating' keto polymorph, more than the full keto polymorph.

Large Stokes shifts can be observed. However, the low intensity of oscillator strengths at long wavelengths reflects the low quantum yield obtained experimentally.[17] The CAM-B3LYP functional performs notably better than the other two in describing the emission features of thermochromic SA. Moreover, it is the only functional providing underestimated λ_{max} for both absorption and emission vertical energies. B3LYP and PBE0 furnish a large redshift, i.e. a large overestimation with respect to the experimental one.

Overall, even if not accurate for vertical excitations, CAM-B3LYP furnishes a better and more balanced estimate of the optical properties of thermochromic SA.

The general trend (i.e. band shifts) shown by the three functionals in Figure 6 reveals a clear dependence on the exchange correlation functional used, less noticeable at short wavelengths. The fundamental difference between CAM-B3LYP and the two global hybrids, i.e. the attenuation of local Coulomb interactions at long-range, seems indeed to be responsible of a better description of the emission features of crystalline SA.

4. Conclusions

We have demonstrated that an ONIOM approach employing a QM/QM' partition and charge embedding provides a fair description of the complex optical features of crystalline thermochromic SA. The emission energies are strongly dependent on the choice of the exchange and correlation functional, the range separated CAM-B3LYP one generally performing better than the tested global hybrids (B3LYP and PBE0).

Nonetheless, systematic shifts in absorption and emission bands optimistically address the potentiality of the present protocol, that need to be refined, mainly, with respect to i) the type of polarization charges; ii) the density functional approximation used for the QM level.

As regards point i), a comparison of polarization models (e.g. Del Re,[52] or Hirshfeld[53]) different from Mulliken,[50] is foreseen.

Furthermore, to confirm the present findings, it would be interesting to explore the performances of this protocol on other molecular crystalline compounds possibly experimentally well characterized.

Acknowledgements

Computational resources for this work were granted by 'Projet 100339' (2013-2014) at GENCI-IDRIS (Orsay, France). This work was supported by the Italian Ministero dell'Istruzione, dell' Università e della Ricerca (MIUR) through the Programma di ricerca di rilevante interesse nazionale" (PRIN) Grant 2010C4R8M8_002 entitled "Nanoscale functional Organization of (bio)Molecules and Hybrids for targeted Application in Sensing, Medicine and Biotechnology" and the ``Futuro in Ricerca" (FIRB) Grant RBFR1248UI 002 entitled "Novel Multiscale Theoretical/Computational Strategies for the Design of Photo and Thermo Responsive Hybrid Organic-Inorganic Components for Nanoelectronic Circuits".

Supporting Information. CAM-B3LYP, B3LYP and PBE0 molecular orbitals (gas-phase and ACN); outputs of all vertical excitation and relaxation energies from the present work.

References:

[1] A. El′tsov, in Organic photochromes; New York, **1990**; Plenum.
[2] V. Ramamurthy, in Photochemistry in organized and constrained media; Wiley-VCH, New York, **1991**.
[3] J. C. Crano, R. J. Guglielmetti, in Organic Photochromic and Thermochromic Compounds; Plenum Press, New York, **1999**.
[4] H. Dürr, H. Bouas-Laurent, in Photochromism: Molecules and Systems; Elsevier, Amsterdam, **2003**; 2nd ed.
[5] M. Irie, *Chem. Rev.*, **2000**, DOI:10.1021/cr980069d.
[6] K. Matsuda, M. Irie, *J. Photochem. Photobiol. C-Photochem. Rev.*, **2004**, DOI:10.1016/j.jphotochemrev.2004.07.003.
[7] M. Ottolenghi, D. S. McClure, *J. Chem. Phys.*, **1967**, DOI:10.1063/1.1840611.
[8] R. V. Andes, D. M. Manikowski, *Appl. Opt.*, **1968**, DOI:10.1364/AO.7.001179.
[9] C. Pasternak, M. Slifkin, M. Shinitzky, *J. Chem. Phys.*, **1978**, DOI:10.1063/1.436101.
[10] J. Lewis, C. Sandorfy, *Can. J. Chem.-Rev. Can. Chim.*, **1982**, DOI:10.1139/v82-237.
[11] T. Sekikawa, T. Kobayashi, T. Inabe, *J. Phys. Chem. A*, **1997**, DOI:10.1021/jp9620126.
[12] M. Y. Shen, L. Z. Zhao, T. Goto, A. Mordzinski, *J. Chem. Phys.*, **2000**, DOI:10.1063/1.480815.
[13] R. G. E. Morales, G. P. Jara, V. Vargas, *Spectrosc. Lett.*, **2001**, DOI:10.1081/SL-100001445.
[14] K. Ogawa, J. Harada, T. Fujiwara, S. Yoshida, *J. Phys. Chem. A*, **2001**, DOI:10.1021/jp003985f.
[15] T. Fujiwara, J. Harada, K. Ogawa, *J. Phys. Chem. B*, **2004**, DOI:10.1021/jp037438g.
[16] V. Vargas, *J. Phys. Chem. A*, **2004**, DOI:10.1021/jp035461w.

[17] M. Ziółek, J. Kubicki, A. Maciejewski, R. Naskręcki, A. Grabowska, *Phys. Chem. Chem. Phys.*, **2004**, DOI:10.1039/B406898J.
[18] W. Rodríguez-Córdoba, J. S. Zugazagoitia, E. Collado-Fregoso, J. Peon, *J. Phys. Chem. A*, **2007**, DOI:10.1021/jp072415d.
[19] J. Harada, T. Fujiwara, K. Ogawa, *J. Am. Chem. Soc.*, **2007**, DOI:10.1021/ja076635g.
[20] M. Sliwa, N. Mouton, C. Ruckebusch, L. Poisson, A. Idrissi, S. Aloïse, L. Potier, J. Dubois, O. Poizat, G. Buntinx, *Photochem. Photobiol. Sci.*, **2010**, DOI:10.1039/B9PP00207C.
[21] T. Sekikawa, O. Schalk, G. Wu, A. E. Boguslavskiy, A. Stolow, *J. Phys. Chem. A*, **2013**, DOI:10.1021/jp4016036.
[22] R. Destro, A. Gavezzotti, M. Simonetta, *Acta Crystallogr. B*, **1978**, DOI:10.1107/S0567740878009449.
[23] F. Arod, P. Pattison, K. J. Schenk, G. Chapuis, *Cryst. Growth Des.*, **2007**, DOI:10.1021/cg060389n.
[24] F. Arod, M. Gardon, P. Pattison, G. Chapuis, *Acta Crystallogr. C*, **2005**, DOI:10.1107/S010827010500911X.
[25] M. H. Luo, H. Y. Tsai, H. Y. Lin, S. K. Fang, K. Y. Chen, *Chin. Chem. Lett.*, **2012**, DOI:10.1016/j.cclet.2012.09.009.
[26] S. Hammes-Schiffer, A. A. Stuchebrukhov, *Chem. Rev.*, **2010**, *110*, 6939–6960.
[27] M. Savarese, P. A. Netti, C. Adamo, N. Rega, I. Ciofini, *J. Phys. Chem. B*, **2013**, DOI:10.1021/jp406301p.
[28] M. Savarese, P. A. Netti, N. Rega, C. Adamo, I. Ciofini, *Phys. Chem. Chem. Phys.*, **2014**, DOI:10.1039/C4CP00068D.
[29] A. Pedone, D. Presti, M. C. Menziani, *Chem. Phys. Lett.*, **2012**, DOI:10.1016/j.cplett.2012.05.049.
[30] D. Presti, A. Pedone, M. C. Menziani, B. Civalleri, L. Maschio, *Crystengcomm*, **2014**, DOI:10.1039/c3ce41758a.
[31] D. Presti, A. Pedone, M. C. Menziani, *Inorg. Chem.*, **2014**, DOI:10.1021/ic5006743.
[32] A. Pedone, G. Prampolini, S. Monti, V. Barone, *Phys. Chem. Chem. Phys.*, **2011**, DOI:10.1039/C1CP21475F.
[33] A. Pedone, J. Bloino, V. Barone, *J. Phys. Chem. C*, **2012**, DOI:10.1021/jp305294u.
[34] M. Z. Zgierski, A. Grabowska, *J. Chem. Phys.*, **2000**, DOI:10.1063/1.1316038.
[35] M. Guillaume, B. Champagne, N. Markova, V. Enchev, F. Castet, *J. Phys. Chem. A*, **2007**, DOI:10.1021/jp074567e.
[36] L. Spörkel, G. Cui, W. Thiel, *J. Phys. Chem. A*, **2013**, DOI:10.1021/jp4028035.
[37] D. Presti, F. Labat, A. Pedone, M. J. Frisch, H. P. Hratchian, I. Ciofini, M. C. Menziani, C. Adamo, *J. Chem. Theory Comput.*, **2014**, DOI:10.1021/ct500868s.
[38] B. Civalleri, C. M. Zicovich-Wilson, L. Valenzano, P. Ugliengo, *Crystengcomm*, **2008**, DOI:10.1039/b715018k.
[39] H. P. Hratchian, P. V. Parandekar, K. Raghavachari, M. J. Frisch, T. Vreven, *J. Chem. Phys.*, **2008**, DOI:10.1063/1.2814164.
[40] P. V. Parandekar, H. P. Hratchian, K. Raghavachari, *J. Chem. Phys.*, **2008**, DOI:10.1063/1.2976570.
[41] M. J. Frisch, G. W. Trucks, H. B. Schlegel, G. E. Scuseria, M. A. Robb, J. R. Cheeseman, G. Scalmani, V. Barone, B. Mennucci, G. A. Petersson, H. Nakatsuji, M. Caricato, X. Li, H. P. Hratchian, A. F. Izmaylov, J. Bloino, G. Zheng, J. L. Sonnenberg, W. Liang, M. Hada, M. Ehara, K. Toyota, R. Fukuda, J. Hasegawa, M. Ishida, T. Nakajima, Y. Honda, O. Kitao, H. Nakai, T. Vreven, J. A. Montgomery, Jr., J. E. Peralta, F. Ogliaro, M. Bearpark, J. J.

Heyd, E. Brothers, K. N. Kudin, V. N. Staroverov, T. Keith, R. Kobayashi, J. Normand, K. Raghavachari, A. Rendell, J. C. Burant, S. S. Iyengar, J. Tomasi, M. Cossi, N. Rega, J. M. Millam, M. Klene, J. E. Knox, J. B. Cross, V. Bakken, C. Adamo, J. Jaramillo, R. Gomperts, R. E. Stratmann, O. Yazyev, A. J. Austin, R. Cammi, C. Pomelli, J. W. Ochterski, R. L. Martin, K. Morokuma, V. G. Zakrzewski, G. A. Voth, P. Salvador, J. J. Dannenberg, S. Dapprich, P. V. Parandekar, N. J. Mayhall, A. D. Daniels, O. Farkas, J. B. Foresman, J. V. Ortiz, J. Cioslowski, and D. J. Fox, in GAUSSIAN09, Revision D.01; Gaussian, Inc., Wallingford CT, **2009**.

[42] R. Dovesi, R. Orlando, B. Civalleri, C. Roetti, V. R. Saunders, C. M. Zicovich-Wilson, *Z. Krist.*, **2005**, DOI:10.1524/zkri.220.5.571.65065.

[43] R. Dovesi, V. R. Saunders, C. Roetti, R. Orlando, C. M. Zicovich-Wilson, F. Pascale, K. Doll, N. M. Harrison, B. Civalleri, I. J. Bush, P. D'Arco, M. Llunell, in CRYSTAL09 User's Manual; Università di Torino, Torino, **2010**.

[44] P. J. Stephens, F. J. Devlin, C. F. Chabalowski, M. J. Frisch, *J. Phys. Chem.*, **1994**, DOI:10.1021/j100096a001.

[45] C. Adamo, V. Barone, *J. Chem. Phys.*, **1999**, DOI:10.1063/1.478522.

[46] T. Yanai, D. P. Tew, N. C. Handy, *Chem. Phys. Lett.*, **2004**, DOI:10.1016/j.cplett.2004.06.011.

[47] A. Pedone, *J. Chem. Theory Comput.*, **2013**, DOI:10.1021/ct4004349.

[48] F. Muniz-Miranda, M. C. Menziani, A. Pedone, *J. Phys. Chem. A*, **2014**, DOI:10.1021/jp507679f.

[49] R. Kobayashi, R. D. Amos, *Chem. Phys. Lett.*, **2006**, DOI:10.1016/j.cplett.2006.04.037.

[50] R. S. Mulliken, *J. Chem. Phys.*, **1955**, DOI:10.1063/1.1740588.

[51] M. Cossi, N. Rega, G. Scalmani, V. Barone, *J. Comput. Chem.*, **2003**, DOI:10.1002/jcc.10189.

[52] G. D. Re, *J. Chem. Soc. Resumed*, **1958**, DOI:10.1039/JR9580004031.

[53] F. L. Hirshfeld, *Theor. Chim. Acta*, **1977**, DOI:10.1007/BF00549096.

Table 1. Computed intramolecular distances (Å) and angles (degrees) for the cis-and trans- keto tautomers of SA in gas-phase and acetonitrile (ACN).

	Gas-Phase (S_1)						**Gas-Phase (S_0)**	
	Cis-keto			Trans-keto			Cis-keto	Trans-keto
	CAM-B3LYP	CIS[a]	OM2/MRCI[b]	CAM-B3LYP	CIS[a]	OM2/MRCI[c]	B3LYP[d]	
N-H	1.040	1.008	1.059	1.014	0.996	-	1.035	1.010
N···O	2.628	-	-	3.888	-	-	2.611	4.095
C-O···H	102.70	-	-	60.37	-	-	103.67	53.77
C5-C6-N-C7	12.83	-	-	11.55	-	-	18.95	15.28
C6-N-C7-C8[e]	179.56	180.00	180.00	-169.27	180.00	-	-179.00	-177.54
O···H	1.756	1.337	1.594	4.446	4.585	-	1.742	4.717
C-O	1.273	1.233	1.268	1.284	1.225	-	1.256	1.233
C7-N	1.339	1.337	1.340	1.342	1.340	-	1.333	1.347
	Solvent ACN (S_1)						**Solvent ACN (S_0)**	
	Cis-keto			Trans-keto			Cis-keto	Trans-keto
	CAM-B3LYP			CAM-B3LYP			B3LYP[d]	
N-H	1.030			1.015			1.032	1.012
N···O	2.684			4.040			2.633	4.095
C-O···H	104.39			55.52			103.22	53.43
C5-C6-N-C7	0.20			4.36			14.85	11.37
C6-N-C7-C8[e]	-179.91			-177.61			-179.05	-178.42
O···H	1.838			4.721			1.774	4.721
C-O	1.271			1.246			1.265	1.246
C7-N	1.349			1.335			1.326	1.335

[a]: from Ref.[34]
[b]: from Ref.[36]
[c]: the trans-keto form was not obtained in Ref.,[36] due to a S_1/S_0 conical intersection.
[d]: B3LYP (optimized S_0) geometries, used as input structures for optimizations in the excited states.
[e]: dihedral angle labeled according to Figure 1. The corresponding one in Ref.[36] is labeled as C6-N7-C8-C9

Table 2. Computed intramolecular distances (Å) and angles (degrees) for the C-cis-keto and C-trans-keto clusters.

	Clusters S_1						Clusters S_0	
	C-cis-keto			C-trans-keto			C-cis-keto	C-trans-keto
	CAM-B3LYP	B3LYP	PBE0	CAM-B3LYP	B3LYP	PBE0	B3LYP-D* [a]	
N-H	1.042	1.045	1.045	1.016	1.017	1.016	1.033	1.014
N···O	2.639	2.658	2.635	3.875	3.868	3.826	2.645	4.021
C-O···H	101.02	99.35	99.60	60.10	60.78	61.61	102.98	55.70
C5-C6-N-C7	24.93	25.85	25.72	3.43	8.86	9.92	2.70	-178.12
C6-N-C7-C8	178.87	179.17	179.20	177.45	177.48	176.95	179.98	178.67
O···H	1.774	1.792	1.763	4.504	4.478	4.43	1.786	4.684
C-O	1.279	1.290	1.282	1.284	1.325	1.31	1.266	1.246
C7-N	1.332	1.331	1.327	1.326	1.334	1.328	1.329	1.335

[a]: B3LYP-D* (optimized S_0) geometries from Ref.,[37] used as input structures for optimizations in the excited states.

Table 3. Absolute difference with respect to the gas phase structure computed for intramolecular distances (Å) and angles (degrees) in ACN and clusters for the cis-keto and trans-keto forms at the CAM-B3LYP level at the excited state.

Abs. differences	**Solvent ACN (S_1)**		**Clusters (S_1)**	
w.r.t. Gas-phase (S_1)	Cis-keto	Trans-keto	**C-cis-keto**	**C-trans-keto**
N-H	0.010	0.001	0.002	0.002
N···O	0.056	0.152	0.011	0.013
C-O···H	1.69	4.85	1.68	0.27
C5-C6-N-C7	12.63	7.19	12.10	8.12
C6-N-C7-C8	0.53	8.34	0.69	13.28
O···H	0.082	0.275	0.018	0.058
C-O	0.002	0.038	0.006	0.000
C7-N	0.010	0.007	0.007	0.016

Table 4. Cis to trans relative stabilities of the keto form optimized at the S_1 excited state, using different exchange correlation functionals (CAM-B3LYP, B3LYP, and PBE0).

	Cis-trans ΔE (kcal/mol per molecule)		
	CAM-B3LYP	B3LYP	PBE0
Gas-phase	-5.92	-4.90	-5.47
ACN solvent	-1.18	-2.50	-2.57
Cluster – no embed	-6.38	-5.71	-6.50
Cluster – embed	-4.02	-4.14	-4.76

Table 5. Computed CAM-B3LYP, B3LYP and PBE0 vertical emission energies. Deviations from experimental data are reported in parentheses. The character and contribution of the most relevant one-electron excitations are also reported.

	Gas-phase				**ACN**			
Method	Cis-keto (nm)	character [a]	Trans-keto (nm)	character	Cis-keto (nm)	character	Trans-keto (nm)	character
CAM-B3LYP	469	0.69 H-L	528	-0.64 H-L 0.29 (H-1)-L	455 (-78/-82)	0.70 H-L	515	0.70 H-L
B3LYP	524	0.68 H-L	610	0.53 H-L -0.46 (H-1)-L	470 (-63/-67)	0.71 H-L	520	0.71 H-L
PBE0	508	0.69 H-L	584	0.55 H-L -0.44 (H-1)-L	459 (-74/-78)	0.71 H-L	507	0.71 H-L
Exp. (ACN)[b]					537			
Exp. (ACN)[c]					533			
	Clusters – no embedding				**Clusters - charge embedding**			
QM/QM'	C-cis-keto (nm)	character	C-trans-keto (nm)	character	C-cis-keto (nm)	character	C-trans-keto (nm)	character
CAM-B3LYP/HF	521 (-20)	-0.68 H-L	533 (-8)	0.67 H-L -0.21 (H-1)-L	509 (-32)	0.69 H-L	527 (-14)	0.68 H-L
B3LYP/HF	669 (+128)	0.68 H-L	683 (+142)	-0.53 H-L 0.47 (H-1)-L	649 (+107)	0.69 H-L	663 (+122)	0.56 H-L -0.43 (H-1)-L
PBE0/HF	631 (+90)	-0.69 H-L	644 (+103)	0.57 H-L -0.42 (H-1)-L	612 (+71)	0.69 H-L	627 (+86)	0.60 H-L 0.38 (H-1)-L
Exp. (crystal)[d]	541		541		541		541	

[a]: H-L and (H-1)-L correspond to HOMO–LUMO and HOMO-1–LUMO one electron excitations, respectively

[b]: from Ref.[18]

[c]: from Ref.[20]

[d]: fluorescence measured on crystal in dried ACN from Ref.,[17] keto emission arbitrarily assigned to both keto forms.

CAPTION TO FIGURES

Figure 1. Scheme of ESIPT and cis-trans tautomerization mechanisms for SA

Figure 2. Pictorial representation of SA in different aggregation states: β crystalline polymorph (enol), **C-enol** cluster, and molecular enol-form (gas-phase). All structures refer to the optimized ground state. The unit cell is shown in purple lines.

Figure 3. Perspective view of the optimized S_1 CAM-B3LYP **C-cis-keto** (left) and **C-trans-keto** (right) clusters. The surrounding molecules (yellow) are in the enol form.

Figure 4. Simulated UV-Visible emission spectra of **C-enol**, **C-cis-keto** and **C-trans-keto** clusters of SA. The spectra computed for the isolated SA molecule in gas-phase and ACN is also reported.

Figure 5. Computed (CAM-B3LYP, B3LYP and PBE0) cis- to trans- keto redshift: the data values have been normalized to a 0%-100% scale. Differences between cis- and trans- keto λ_{max} (nm) are reported (see also Supporting Information).

Figure 6. Molecular Orbitals computed for cis- and trans- keto tautomers in gas-phase (B3LYP level on optimized S_1 structure).

Figure 7. Simulated absorption (full line) and fluorescence (dashed line) spectra from result obtained using a QM/QM' + charge embedding model. Cis- and trans- keto absorption λ_{max} from Ref.[15]; steady-state keto emission of the crystal in dried ACN λ_{max} from Ref.[17]

FIGURE 1

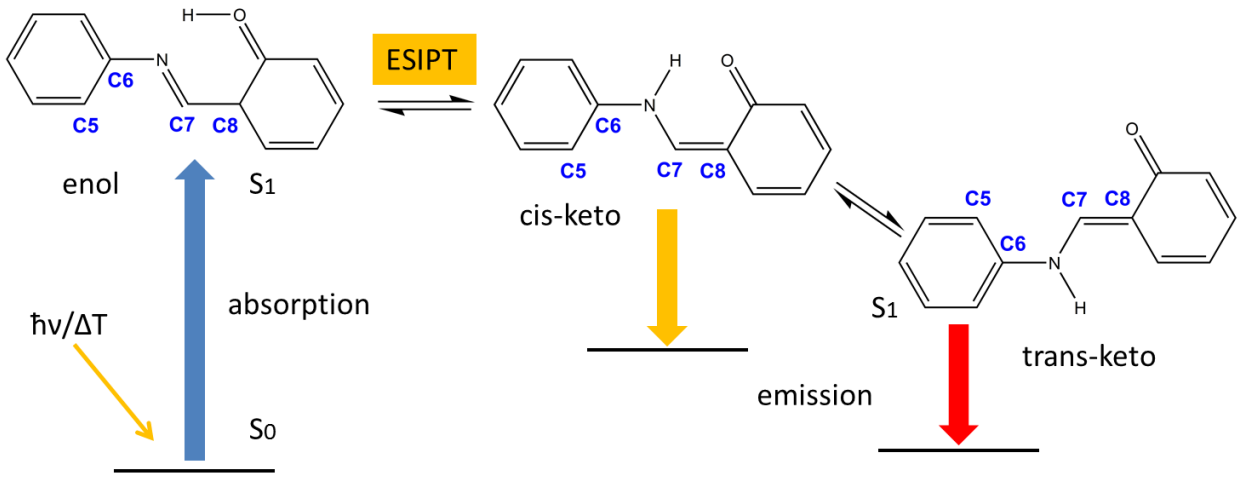
ESIPT
enol
S1
absorption
ħv/ΔT
S0
cis-keto
emission
trans-keto
C5
C6
C7
C8
N
H
O

FIGURE 2

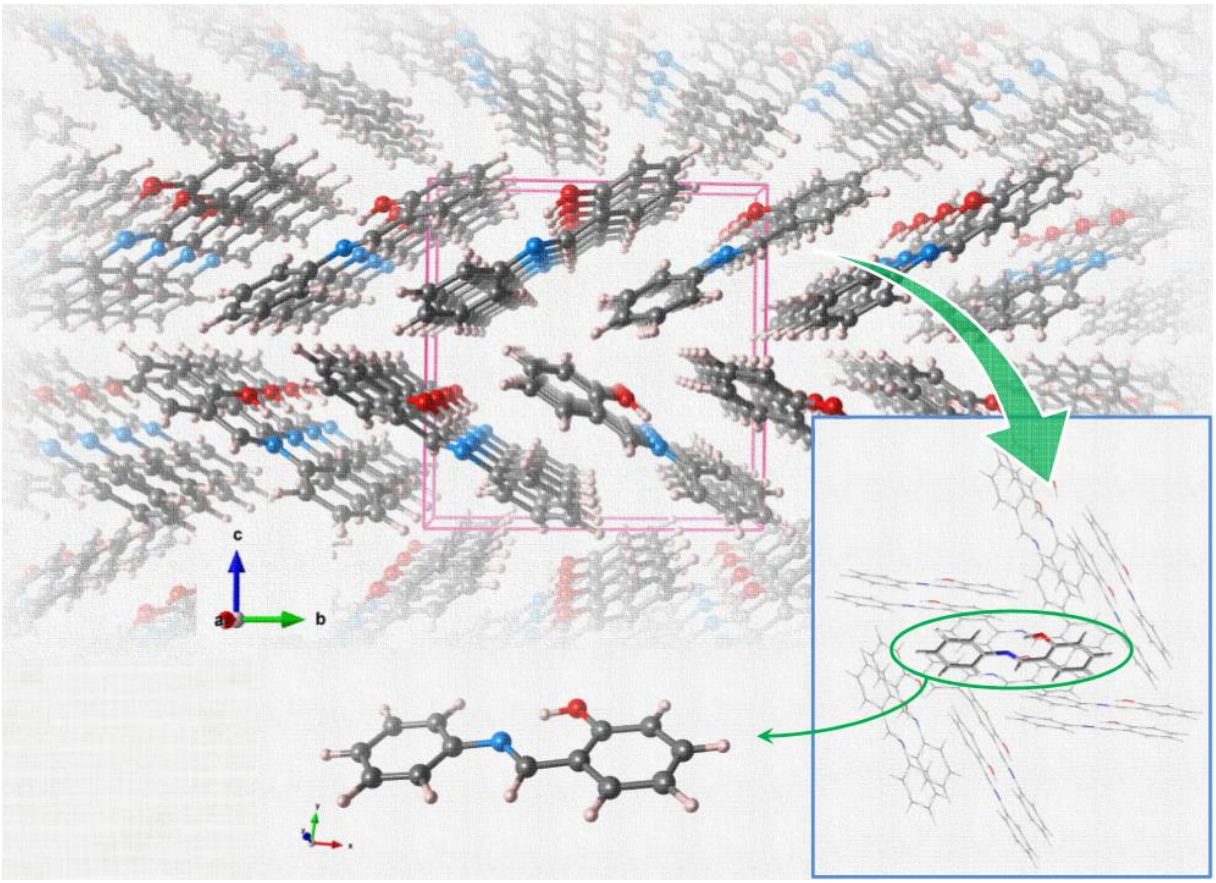

FIGURE 3

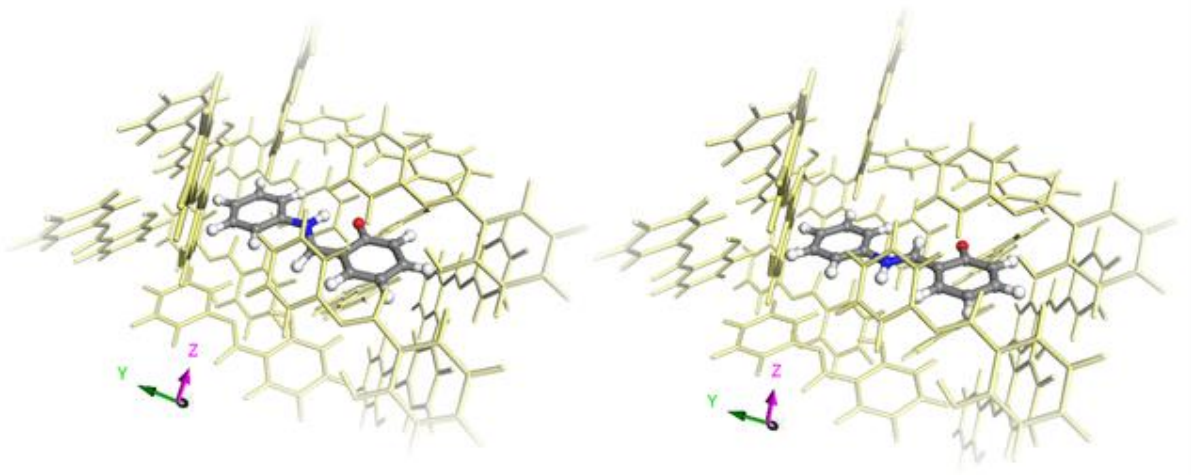

FIGURE 4

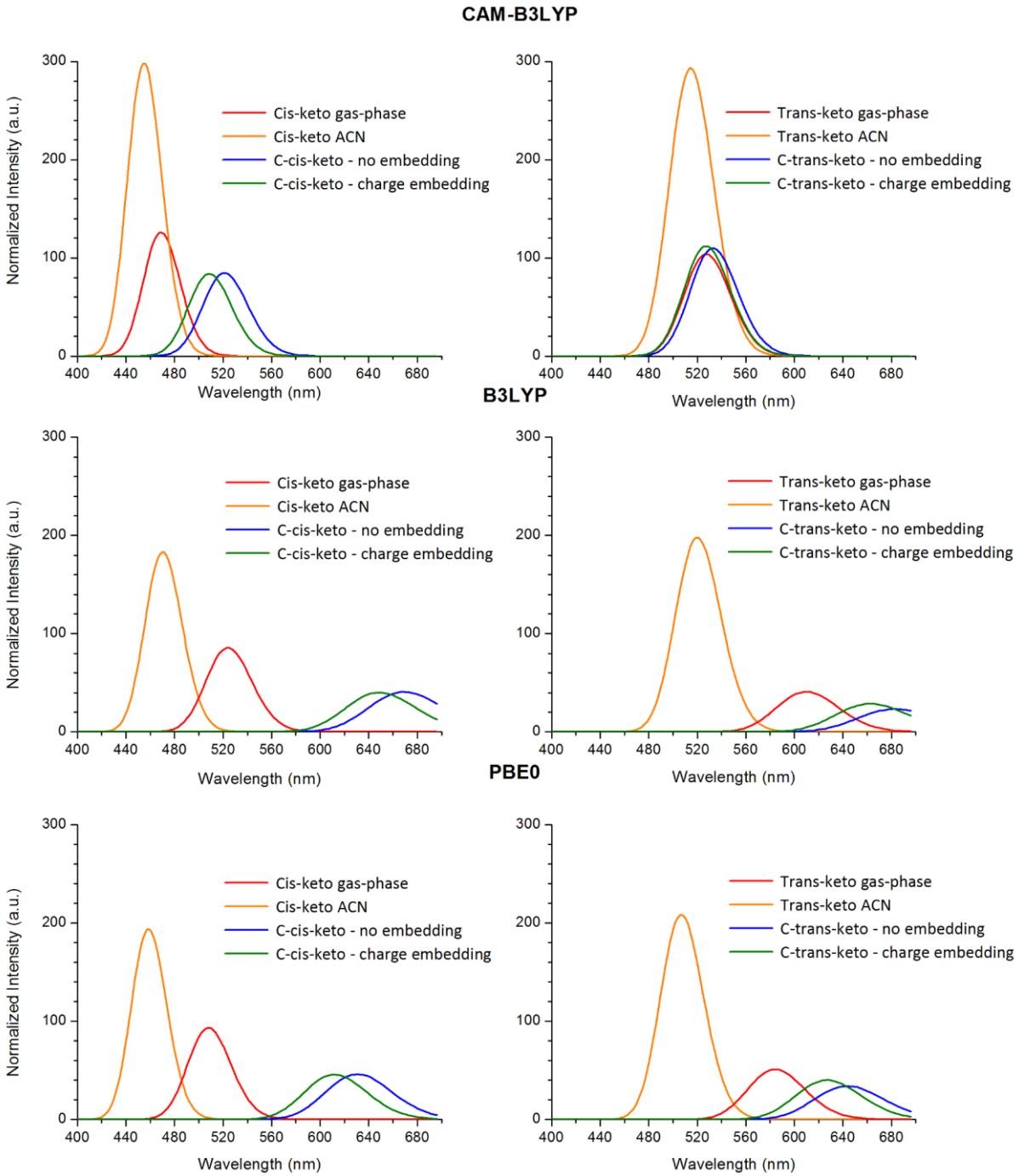
CAM-B3LYP
B3LYP
PBE0
Normalized Intensity (a.u.)
Wavelength (nm)
Cis-keto gas-phase
Cis-keto ACN
C-cis-keto - no embedding
C-cis-keto - charge embedding
Trans-keto gas-phase
Trans-keto ACN
C-trans-keto - no embedding
C-trans-keto - charge embedding

FIGURE 5

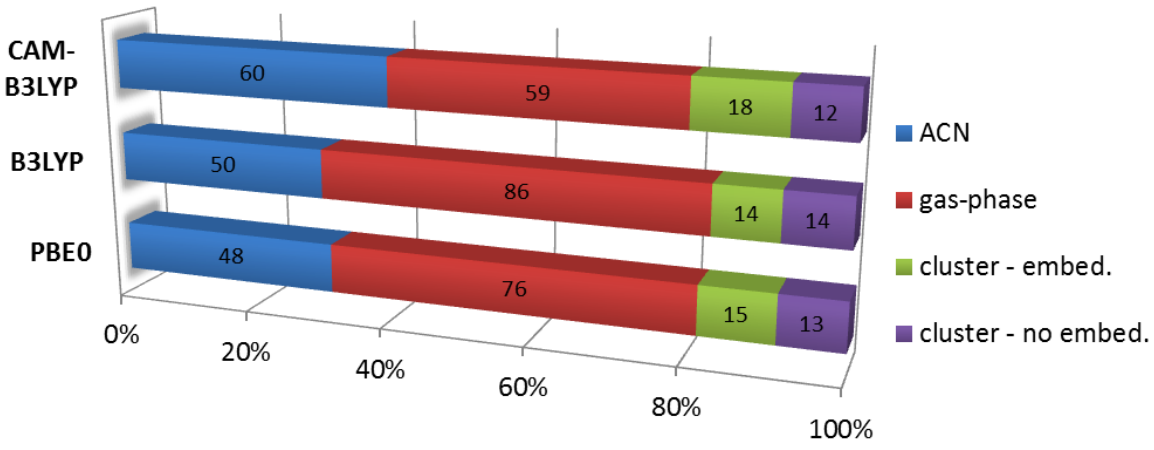
CAM-B3LYP
B3LYP
PBE0
60
59
18
12
50
86
14
14
48
76
15
13
0%
20%
40%
60%
80%
100%
ACN
gas-phase
cluster - embed.
cluster - no embed.

FIGURE 6

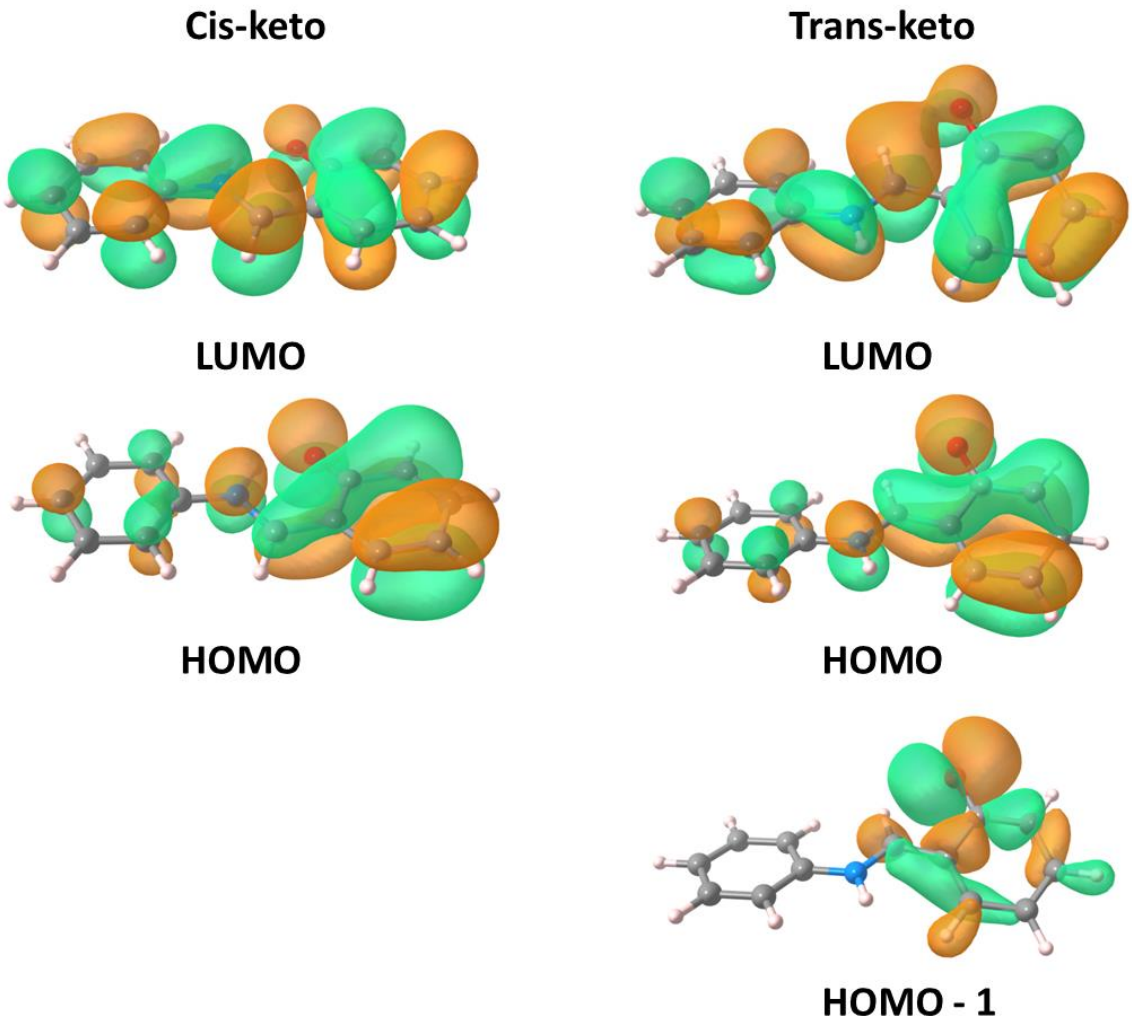

FIGURE 7

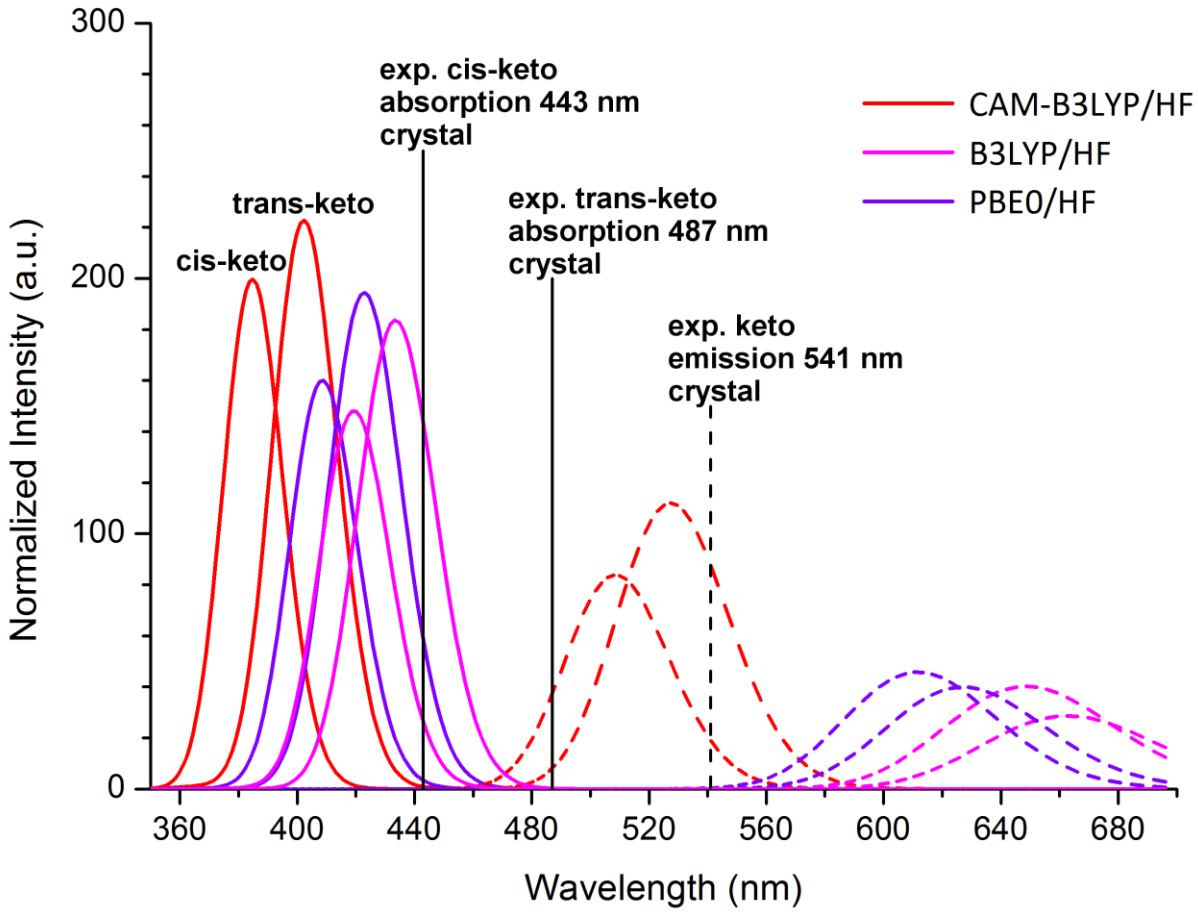
300
200
100
0
Normalized Intensity (a.u.)
360
400
440
480
520
560
600
640
680
Wavelength (nm)
exp. cis-keto
absorption 443 nm
crystal
trans-keto
cis-keto
exp. trans-keto
absorption 487 nm
crystal
exp. keto
emission 541 nm
crystal
CAM-B3LYP/HF
B3LYP/HF
PBE0/HF

TOC GRAPHICS